Mechatronic Design of an Active Two-body Vibration Isolation System

E. Csencsics, M. Thier, P. Siegl, G. Schitter

Automation and Control Institute, Vienna University of Technology, Gusshausstrasse 27-29, 1040 Vienna, Austria (e-mail: csencsics@acin.tuwien.ac.at).

Abstract:
Structural modes as for example decoupling of a mechanical subsystem are in general unwanted effects in high precision positioning systems. This paper proposes a well designed decoupling mechanism as a design choice to improve the energy efficiency of an active vibration isolation system that needs to position a structure comprising a high and low precision subsystem. Experimental setups of a single DoF system with a rigid and a decoupling mechanical system structure are developed and analyzed. PD and a PID controllers are designed for the rigid and the equivalent decoupling structure, respectively, resulting in the same disturbance rejection performance for the high precision subsystem. Experiments demonstrate that disturbances of 12.4 μm rms amplitude are reduced to below 118 nm rms for both systems and that the rms energy consumption of the decoupling structure can be reduced by 68% as compared to the rigid system structure.

Keywords: Vibration isolation, Systems design, Mechanical decoupling, PID controllers, Reduced energy consumption

1. INTRODUCTION

High precision positioning systems in production and metrology often require high control bandwidths to ensure the required levels of precision (Munnig Schmidt et al. (2014)). External vibrations are a common problem for these tasks, as they are in general sensitive to disturbances (Amick et al. (2005)). In literature thus numerous passive (Carrella et al. (2007)) and active vibration isolation systems (Kim et al. (2009)), equipped with sensors and actuators to actively reject external vibrations, are commonly proposed countermeasures in these fields. Active concepts that maintain constant proximity between a probe and a sample by means of closed loop control are also reported (Thier et al. (2015), Ito et al. (2015)).

Structural modes of the positioned structure represent a challenge for such active closed loop controlled concepts, as they in general may limit the achievable closed loop bandwidth. Structural modes originate either from modes of the individual components of the positioned structure or their interconnections, as in the case of a decoupling sub-mass (Munnig Schmidt et al. (2014)). Almost every structure that can be considered rigid at low frequencies shows internal structural modes, meaning additional system dynamics, at higher frequencies, depending on its shape and density. There are different strategies proposed in literature to cope with structural modes ranging from active damping (Babakhani and De Vries (2010)) and over-actuation (Schneiders et al. (2003), Falangas et al. (1994)), to the appropriate placement of actuators (Nestorovic and Trajkov (2013)). All of them, however, require an increased system complexity or a high system analysis effort.

In contrast to active concepts structural modes, such as decoupling sub-systems, are intentionally used in passive vibration isolation systems. Applications proposed in Giaime et al. (1996) and Pirro (2006) use passive vibration isolation stacks to reduce the transmissibilty of the resulting structure and to isolate sensitive equipment from ground vibrations. In Csencsics et al. (2016) it is shown that a well designed decoupling mechanism can also be introduced in an active vibration isolation system to improve versatility, without impairing the controllability of the system.

This paper presents the advantage of a designed decoupling mechanism introduced in an active vibration isolation system that positions a structure comprising a high and a low precision subsystem in constant distance to a reference. The proposed approach offers the design freedom to reduce the overall energy consumption of the system for high bandwidth positioning of the high precision subsystem. To demonstrate this targeted property the system design and the experimental setup of a rigid system concept with a high and a low precision sub-metrology-system is presented and analyzed in Section 2. Section 3 introduces the developed single axis prototype of a two-body system design with decoupling mechanism and provides a thorough system analysis. Based on the identification data PD and PID controllers are designed in Section 4 for the rigid and the decoupling system, respectively. In Section 5 it is demonstrated that the control effort for high bandwidth control of the high precision subsystem can be significantly reduced in the system with decoupling mechanism, while maintaining an equal disturbance rejection performance as in the rigid system. Section 6 concludes the paper.

Post-print version of the article: Ernst Csencsics, Markus Thier, Philip Siegl and Georg Schitter, "Mechatronic Design of an Active Two-body Vibration Isolation System," *Proceedings of the 7th IFAC Symposium on Mechatronic Systems*, pp. 133-140, 2016. DOI: 10.1016/j.ifacol.2016.10.532

2. RIGID SYSTEM DESIGN AND IDENTIFICATION

2.1 System description and modeling

In Fig. 1 the concept of a high precision metrology system which is positioned in constant distance Δz to a measurement sample is shown. It comprises a lightweight sub-metrology-system MS1 which requires high precision and bandwidth and a heavy sub-metrology-system MS2 requiring only low precision and bandwdith. Both sub-metrology-systems are mounted on a rigid metrology platform with an entire mass $m_{1,2}$ (platform plus sub-metrology-systems). The platform is connected to mechanical ground via the actuator suspension (k_1 and d_1) and actuated via the force F. It is subject to external ground vibrations, which disturb the constant distance Δz to the sample. The coordinate $z_{1,2}$ represents the vertical position of the platform body.

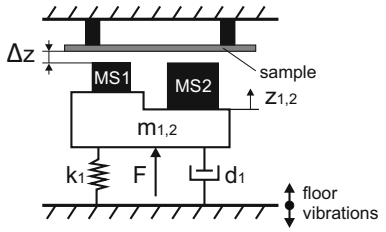

Fig. 1. Mechanical model of the rigid system design concept of a high precision metrology system that is positioned in constant distance to a sample. The high precision subsystem MS1 and the low precision subsystem MS2 are stiffly mounted to the metrology platform (rigid body). $m_{1,2}$ represents the mass of the entire metrology platform and is connected to mechanical ground via the actuator suspension (k_1 and d_1) and actuated by force F.

To model the dynamics of the rigid system along a single degree of freedom the lumped mass models in Fig. 1 is considered. The differential equation, describing the motion of the body of the rigid system, is

$$m_{1,2}\ddot{z}_{1,2}(t) = F - k_1 z_{1,2}(t) - d_1 \dot{z}_{1,2}(t). \tag{1}$$

The transfer function (TF) from the applied force F to the vertical position $z_{1,2}$ can be obtained by reordering (1) and applying the Laplace transformation. This results in the second order TF:

$$G_R(s) = \frac{Z_{1,2}(s)}{F(s)} = \frac{1}{m_{1,2}s^2 + d_1 s + k_1}. \tag{2}$$

To fulfill the requirements on disturbance rejection for both subsystems in closed loop control, the entire platform mass $m_{1,2}$ needs to be actuated over the entire frequency range, that is required to reach the high precision requirements of MS1. Especially for platforms with large mass and target cross over frequencies of several hundred Hertz this might quickly exceed the capabilities of the power amplifier or the actuator in terms of maximum rms current. This can impose stringent requirements of the platform weight, require unnecessary large actuators or high current power amplifiers, or even trouble the feasibility of the targeted system bandwidth and precision requirements.

2.2 Experimental setup

The rigid system structure in the experimental setup is composed of a solid aluminium block ($m_{1,2}$=5.7 kg). It is placed directly on the mover of a voice coil actuator (Shaker S51110, TIRA GmbH, Germany) that is placed on mechanical ground and used for vertical actuation. The actuator is driven by a custom made current amplifier (Amplifier type MP38CL, Apex Microtechnology, Tucson, AZ, USA). The amplifier is controlled by a current controller with a bandwidth of 10 kHz, implemented on the FPGA of a dSpace-platform (Type: DS1005, dSPACE GmbH, Germany). The controller implementation is done on the processor of the dSpace-platform running at a sampling frequency of 20 kHz.

For measuring the position $z_{1,2}$ of the mass $m_{1,2}$ an eddy current sensor S_E (eddyNCDT DT3702-U1-A-C3, Micro-Epsilon GmbH, Germany) is used. The input of the system is the input of the current amplifier, which via the motor constant exerts a force on the moving mass. The signal of the position sensor is considered as the system output.

2.3 System identification

The frequency response is measured by applying a sine sweep and measuring magnitude and phase response by the Lock-In principle with the dSPACE-platfrom (Masciotti et al. (2008)). The measured frequency responses of the rigid system is depicted in Fig. 2. The 2nd order mass-

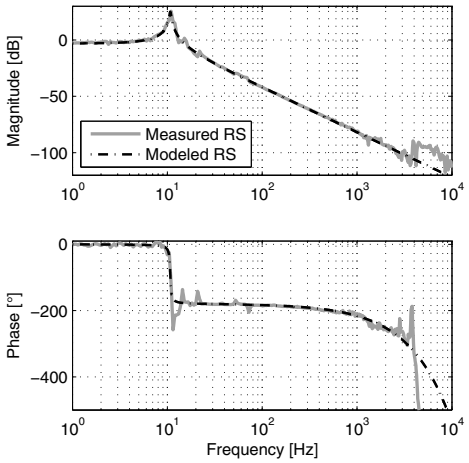

Fig. 2. Measured and modeled frequency response of the rigid system (RS). The frequency response shows mass-spring dynamics resulting from the rigid mass and the actuator suspension with a suspension mode at 11 Hz.

spring characteristic with a suspension mode at 11 Hz and a -40 dB slope after this frequency is clearly visible. Fig. 2 additionally shows the system model

$$G_{RS}(s) = K \cdot G_R(s), \tag{3}$$

with K=1.686e4, $G_R(s)$ according to (2) and coefficients according to Table 1, which is fitted to the measured data.

Post-print version of the article: Ernst Csencsics, Markus Thier, Philip Siegl and Georg Schitter, "Mechatronic Design of an Active Two-body Vibration Isolation System," *Proceedings of the 7th IFAC Symposium on Mechatronic Systems*, pp. 133-140, 2016. DOI: 10.1016/j.ifacol.2016.10.532

The sampling delay of T_s=50μs of the digital system is also included in the system model. It can be seen that for target cross over frequencies between 200 Hz and 2 kHz the controller already needs to lift the mass line of the system between 50 and 100 dB.

Table 1. Coefficients for the system model of the rigid system.

Parameter	Value	Unit
$m_{1,2}$	5.7	kg
k_1	25e3	N/m
d_1	13	N·s/m

3. DECOUPLING SYSTEM DESIGN AND IDENTIFICATION

3.1 System description and modeling

Considering that the entire metrology system is composed of two functionally decoupled sub-metrology-systems, one with high (MS1) and one with low (MS2) precision requirements, a mechanical decoupling mechanism is introduced between the two subsystems. Due to this decoupling mechanism the heavy low precision subsystem MS2 decouples at a designed frequency from the lightweight high precision subsystem MS1, which is directly mounted to the actuator. The decoupling frequency is chosen such that the precision requirements on MS2 are met. Above the decoupling frequency only the mass of the subsystem with MS1 remains for positioning, due to the decoupling of the subsystem with MS2. This makes a targeted high cross over frequency, to fulfill the high precision requirements of MS1, even for heavy platforms feasible, without running into current limitations. A needed change of the actuator, the power amplifier or the entire platform weight and design can thus be avoided.

Fig. 3 shows the concept of the metrology system with decoupling mechanism. For the decoupling system the mass of the entire platform $m_{1,2}$ of the rigid system is distributed over the high precision inner body with m_1 and the low precision outer body with m_2 ($m_{1,2}$=m_1+m_2). The inner body is directly attached to the actuator and actuated by the force F. It is connected to mechanical ground via the actuator suspension k_1 and d_1. Both subsystems are connected via spring k_2 and damper d_2, representing the dynamics of the designed decoupling mechanism (grey area in Fig. 3). The coordinate z_1 represents the vertical position of the inner body. In contrast to the rigid system only the body with m_1 needs to fulfill the precision and bandwidth requirements of MS1.

For modeling the dynamic behavior of the decoupling system along a single degree of freedom the lumped mass model in Fig. 3 is considered. The differential equations, describing the motion of the inner body with m_1 and the outer body with m_2, are

$$\begin{aligned} m_1\ddot{z}_1(t) = F &- k_1 z_1(t) - k_2(z_1(t) - z_2(t)) \\ &- d_1\dot{z}_1(t) - d_2\left(\dot{z}_1(t) - \dot{z}_2(t)\right), \end{aligned} \tag{4}$$

and

$$m_2\ddot{z}_2(t) = k_2(z_1(t) - z_2(t)) + d_2\left(\dot{z}_1(t) - \dot{z}_2(t)\right). \tag{5}$$

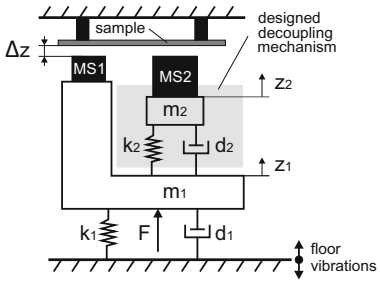

Fig. 3. Mechanical model of the dual body mass-spring-damper system of a design concept of a high precision metrology system with decoupling mechanism. The former rigid metrology platform is distributed over two coupled parts. The high precision subsystem MS1 with mass m_1 is connected to mechanical ground via the actuator suspension (k_1 and d_1) and actuated by force F. The low precision subsystem MS2 with mass m_2 is connected to MS1 via the designed decoupling mechanism comprising k_2 and d_2.

The TF from the applied force F to the vertical positions z_1 is obtained by combining (4) and (5), and by applying the Laplace transformation, resulting in

$$G_D(s) = \frac{Z_1(s)}{F(s)} = \frac{m_2 s^2 + d_2 s + k_2}{m_1 m_2 s^4 + D_3 s^3 + D_2 s^2 + D_1 s + k_1 k_2}, \tag{6}$$

with

$$D_1 = d_1 k_2 + d_2 k_1, \tag{7}$$
$$D_2 = d_1 d_2 + k_1 m_2 + k_2 m_1 + k_2 m_2, \tag{8}$$
$$D_3 = d_1 m_2 + d_2 m_1 + d_2 m_2. \tag{9}$$

3.2 Experimental setup

The experimental setup of the decoupling system structure is shown in Fig. 4. It is composed of an inner solid aluminium block (m_1=1.4 kg) and an outer aluminium frame (m_2=4.3 kg) connected by a designed spring-damper decoupling mechanism (Csencsics et al. (2016)). The inner block of the mechanical structure is mounted on the actuator mover. The input of the system is the input of the current amplifier. The position sensor is used to measure the position z_1 of the inner body with mass m_1, which is the considered as system output.

3.3 System Identification

The measured frequency response of the decoupling system is depicted in Fig. 5. It shows the same dynamics as the rigid system up to 60 Hz, with a suspension mode at 11 Hz and a -40 dB slope above this frequency. It further shows a damped anti-resonance and resonance at f_a=78 Hz and f_r=170 Hz, due to the decoupling mass m_2. Above the decoupling only the mass m_1 of the inner body remains for positioning. To demonstrate good accordance with theory, Fig. 5 additionally shows the system model

$$G_{DS}(s) = K \cdot G_D(s), \tag{10}$$

with K=1.686e4, $G_D(s)$ according to (6) and coefficients according to Table 2, which is fitted to the measured data.

Post-print version of the article: Ernst Csencsics, Markus Thier, Philip Siegl and Georg Schitter, "Mechatronic Design of an Active Two-body Vibration Isolation System," *Proceedings of the 7th IFAC Symposium on Mechatronic Systems*, pp. 133-140, 2016. DOI: 10.1016/j.ifacol.2016.10.532

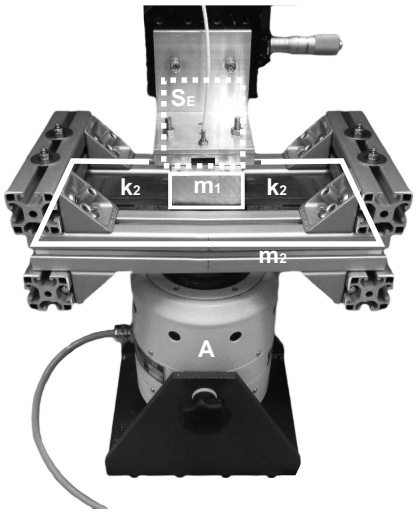

Fig. 4. Experimental lab setup of the decoupling system. The inner body with m_1 and the outer body with m_2 are depicted. A is the actuator, S_E is the eddy current sensor that measures the position z_1 and k_2 are the leaf springs of the decoupling mechanism.

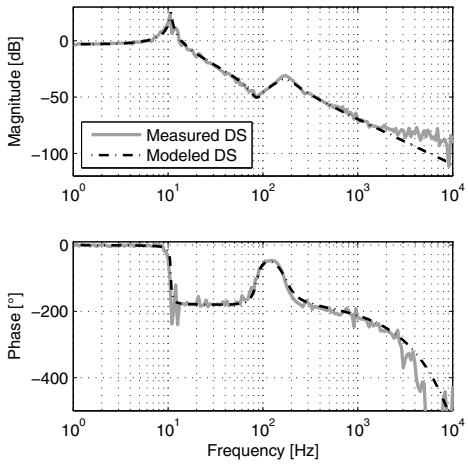

Fig. 5. Measured and modeled frequency response of the decoupling system (DS). The frequency response shows the same mass-spring dynamics as the rigid system up to 60 Hz with a suspension mode at 11 Hz. It further shows a well damped decoupling anti-resonance resonance combination at f_a=78 Hz and f_r=170 Hz, respectively.

The sampling delay (T_s=50μs) of the digital system is again included.

Fig. 6 shows a comparison of the magnitude plots of the measured frequency responses of the rigid and the decoupling system. It can be seen that due to the decoupling of the mass m_2 the mass line after the decoupling frequency

Table 2. Coefficients for the system model of the decoupling system.

Parameter	Value	Unit
m_1	1.4	kg
m_2	4.3	kg
k_1	25e3	N/m
k_2	13e5	N/m
d_1	13	N·s/m
d_2	400	N·s/m

is vertically lifted. Due to the ratio of entire mass m_1+m_2 to the mass m_1 the mass line of the decoupling system is in this area 12 dB higher than the one of rigid system. This suggests that for the decoupling system the same cross over frequency of the controlled inner high precision body can be achieved with less control effort (see Section 4.1).

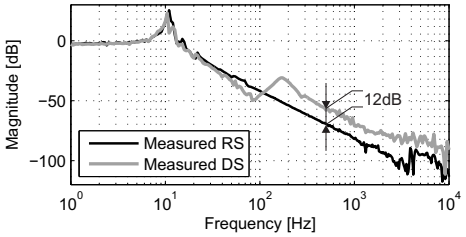

Fig. 6. Comparison of the magnitude plots of the measured frequency responses of the rigid (RS) and the decoupling system (DS). The magnitude plot of the decoupling system (grey) shows that at f_r=170 Hz the mass m_2 decouples, leaving only the mass m_1 for high bandwidth positioning. The reduced mass leads to a lift of the mass line of 12 dB with respect to the magnitude plot of the rigid system (black).

4. CONTROLLER DESIGN

To allow a comparison of the consumed energy an equally good disturbance rejection performance for the body with $m_{1,2}$ of the rigid system and the high precision part (inner body) with m_1 of the decoupling system is targeted. Feedback controllers are thus designed for both systems. The target open loop bandwidth of the systems is set to 600 Hz in order to achieve good disturbance rejection and to avoid an increased controller order in order to deal with the anti-resonance of the decoupling system.

As the suspension mode of the rigid system lies at 11 Hz and the dynamics are dominated by the mass line above this frequency, a tamed PD controller is designed according to Munnig Schmidt et al. (2014). The P-gain shifts the intersection of the mass- and 0 dB-line to the targeted cross over frequency, while the D-gain is chosen to maximize the phase lead at the cross over frequency, resulting in a phase margin of 36°. A realization term stops the differential action at a frequency of 1.8 kHz to limit the control effort at higher frequencies. This results in a first order controller of the form

$$C_{RS} = K_{RS}\frac{s+\omega_{z,RS}}{s+\omega_{p,RS}} \tag{11}$$

with K_{RS}=1.07e3, $\omega_{z,RS}$=1.26e3 and $\omega_{p,RS}$=1.131e4.

Post-print version of the article: Ernst Csencsics, Markus Thier, Philip Siegl and Georg Schitter, "Mechatronic Design of an Active Two-body Vibration Isolation System," *Proceedings of the 7th IFAC Symposium on Mechatronic Systems*, pp. 133-140, 2016. DOI: 10.1016/j.ifacol.2016.10.532

The targeted cross over bandwidth and the decoupling resonance are well separated, such that the C_{RS} with an adjusted DC-gain, to account for the lifted mass line, is taken as starting point. To ensure an equal disturbance rejection performance at low frequencies, where both plant TFs are equal, a tamed integrating action between 50 Hz and 200 Hz is added, that results in an equal DC level for both controllers. This results in a tamed PID controller of the form

$$C_{DS} = K_{DS}\frac{(s+\omega_{z,DS})^2}{(s+\omega_{p1,DS})(s+\omega_{p2,DS})} \tag{12}$$

with K_{DS}=275.12, $\omega_{z,DS}$=1.26e3, $\omega_{p1,DS}$=1.131e4 and $\omega_{p2,DS}$=307.87.

A test signal complying to the BBN VC-A criterion, see Ungar and Gordon (1983), is used to experimentally evaluate the disturbance rejection performance. Thus the equality of the sensitivity functions of both system is verified in simulation up front using the power spectral density (PSD) defined by the criterion.

4.1 Controller implementation

Both controllers are discretized using *Pole-Zero-Matching*, see Franklin et al. (1997), for a sampling frequency f_s=20 kHz, where poles and zeros are directly transformed by $z = e^{s/f_s}$. The measured controller TFs of both controllers are depicted in Fig. 7.

It shows that at frequencies below 30 Hz the gains of both controllers are equal, to achieve an equal disturbance rejection performance in this range where both plant TFs are still identical. At 50 Hz the integrator of C_{DS} starts and lowers the gain of C_{DS} compared to C_{RS}. The D-action starts for both controllers at 200 Hz resulting in a 14° reduced phase lead of the C_{DS} at the targeted cross over frequency. Above the decoupling frequency f_r only the mass of the inner body is left for positioning, such that the gain of C_{DS} can be 12 dB smaller than the gain of C_{RS}, resulting in an reduced control effort.

5. EXPERIMENTAL RESULTS

The measured open loop TFs of the rigid and the decoupling system with the related controllers are depicted in Fig. 8. Both TFs show a cross over frequency of 650 Hz with phase margins of 36° and 25° and gain margins of 8.8 dB and 6.8 dB, respectively.

The measured sensitivity functions of the rigid and the decoupling system are shown in Fig. 9. At frequencies below 20 Hz both sensitivity functions are equal, while the decoupling system lies above the rigid system between 20 Hz and 100 Hz and below it between 100 Hz and the cross over frequency. This behavior results from the decreased and increased loop gain around the decoupling anti-resonance and resonance, respectively. Both sensitivity functions cross the 0 dB line around 400 Hz and attain peaks of 12.5 dB (RS) and 9.7 dB (DS), due to the *Waterbed effect* (Preumont (2012)). Between 1 kHz and 3 kHz the sensitivity function of the rigid system lies below the sensitivity function of the decoupling system.

The evaluation of the disturbance rejection performance in the time domain and the energy consumption is done

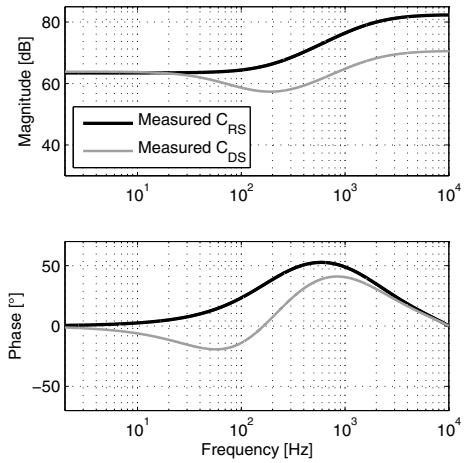

Fig. 7. Measured frequency response of the rigid and decoupling system controller C_{RS} and C_{DS}. C_{RS} is a tamed PD controller designed for an open loop cross over frequency of 600 Hz with the rigid system. C_{DS} is a tamed PID controller, tuned to result in an equal bandwidth and disturbance rejection performance with the decoupling system.

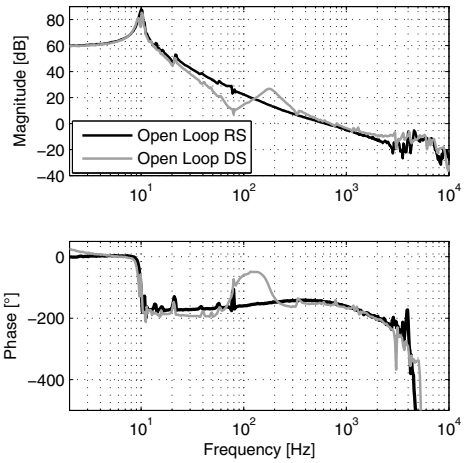

Fig. 8. Measured open loop TFs of the rigid (black) and the decoupling system (grey) with the related controllers. Both show cross over frequencies around 650 Hz and phase margins of 36° (RS) and 25° (DS).

by applying a disturbance profile that satisfies the spectral BBN VC-A criterion, see Ungar and Gordon (1983), as reference, while the error signal is considered as output. This relation results in an equal TF as the output-disturbance to output relation. Fig. 10 shows the results for both systems. The positioning error of the rigid system shows a peak-to-peak value of 1.26 μm and a rms value of 116 nm with an rms current value of 513 mA. The decoupling

Post-print version of the article: Ernst Csencsics, Markus Thier, Philip Siegl and Georg Schitter, "Mechatronic Design of an Active Two-body Vibration Isolation System," *Proceedings of the 7th IFAC Symposium on Mechatronic Systems*, pp. 133-140, 2016. DOI: 10.1016/j.ifacol.2016.10.532

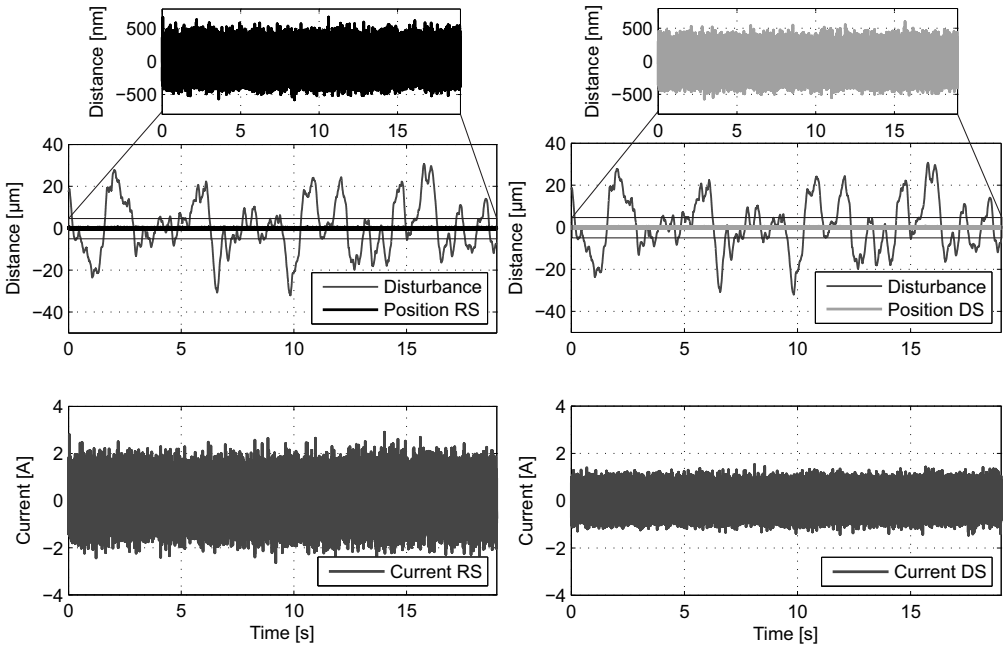

(a) Rigid system TF. (b) Decoupling system TF.

Fig. 10. Disturbance rejection and current evaluation of the closed loop rigid (RS) and the decoupling system (DS). The disturbance with 62.8μm peak-to-peak and 12.4μm rms value is applied and the error is evaluated. (a) shows the error of the rigid system with 1.26μm peak-to-peak and 116 nm rms value. The rms current is 513 mA. (b) shows the error of the decoupling system with 1.17μm peak-to-peak and 118 nm rms value. The rms current is 292 mA.

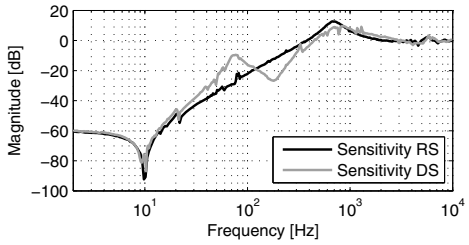

Fig. 9. Measured sensitivity functions of the closed loop rigid (black) and decoupling system (grey). At frequencies below 20 Hz both sensitivity functions are equal. Between 20 Hz and the cross over the sensitivity function of the decoupling system lies first above and then below the one of the rigid system, respectively. Both cross the 0 dB line around 400 Hz.

system offers an equal disturbance rejection performance with a peak-to-peak error value of 1.17 μm and a rms value of 118 nm. The rms current value is 292 mA and thus 43% smaller than in the case of the rigid system. This denotes a reduction of the energy consumption by 68%.

Additionally providing a frequency domain analysis of the time signals, Fig. 10 and Fig. 11 show the power spectral densities (PSDs) of the disturbance signal and the tracking error of the rigid and the decoupling system. At frequencies below 10 Hz both disturbance PSDs are

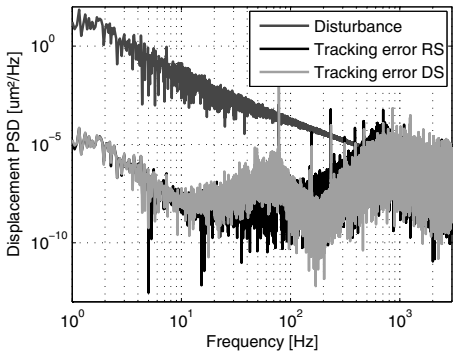

Fig. 11. Power spectral density (PSD) of the disturbance and the error signal of the rigid (RS) and the decoupling system (DS). The error components are equal except around the decoupling aanti-resonance/resonance and match the shape of the sensitivity function.

attenuated by six orders of magnitude, which corresponds to the −60 dB of the sensitivity functions. Around the decoupling anti-resonance/resonance a difference in the error spectra comparable to the different shapes of the sensitivity functions is observable. After a peak of the decoupling system at about 70 Hz and a valley just

Post-print version of the article: Ernst Csencsics, Markus Thier, Philip Siegl and Georg Schitter, "Mechatronic Design of an Active Two-body Vibration Isolation System," *Proceedings of the 7th IFAC Symposium on Mechatronic Systems*, pp. 133-140, 2016. DOI: 10.1016/j.ifacol.2016.10.532

below 200 Hz both error spectra approach the disturbance spectrum at frequencies above 1 kHz, as disturbances at these frequencies can not be rejected (compare Fig. 9).

The PSDs of the current signals are shown in Fig. 12. The spectrum corresponds to the spectrum of the disturbance weighted with the input sensitivity function $U(s) = C(s)/(1 + G(s)C(s))$ of the respective system. It can be seen that at frequencies above the decoupling resonance the current components of the decoupling system are significantly smaller than the current components of the rigid system.

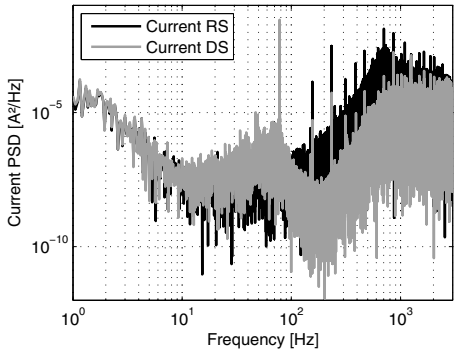

Fig. 12. Power spectral density (PSD) of the current signal at the controller output of the rigid (RS, black) and decoupling system (DS, grey). The current components above the decoupling resonance of 190 Hz are significantly smaller in the case of the DS signal.

In summary it is shown that by introduction of a mechanical decoupling mechanism the energy consumption in the closed loop controlled system can be reduced by a factor of 68% as compared to a rigid structure, while maintaining an equal disturbance rejection performance of the high precision subsystem.

6. CONCLUSION

In this paper a mechanically decoupling mechanism is proposed as a design choice to reduce the energy consumption in an active vibration isolation system composed of a lightweight subsystem with high precision requirements and a heavy subsystem with low precision requirements. It is shown that by introducing a well-damped decoupling mechanism (in this case at 170 Hz) into the initially rigid system strucutre and applying the designed PID controller the rms current can be reduced by 43% as compared to the original rigid system with the designed PD controller. This equals an reduced energy consumption of 68% and can be obtained while still maintaining the same disturbance rejection performance for the high precision subsystem. As introduced this principle can be used in an energy efficient design of metrology platforms that carry two metrology systems with different requirements. Future work focuses on the implementation of the decoupling mechanism in systems with 3 degrees of freedom.

ACKNOWLEDGEMENTS

The authors acknowledge funding from the EU commission under the FP7 NMP Program, project title aim4np, grant number 309558.

REFERENCES

Amick, H., Gendreau, M., Busch, T., and Gordon, C. (2005). Evolving criteria for research facilities: vibration. *Optics & Photonics 2005*, 593303.

Babakhani, B. and De Vries, T.J. (2010). Active damping of the 1d rocking mode. *International Conference on Mechatronics and Automation (ICMA), IEEE*, 1370–1375.

Carrella, A., Brennan, M., and Waters, T. (2007). Static analysis of a passive vibration isolator with quasi-zero-stiffness characteristic. *Journal of Sound and Vibration*, 301(3), 678–689.

Csencsics, E., Thier, M., Hainisch, R., and Schitter, G. (2016). System and control design of a voice coil actuated mechanically decoupling two-body vibration isolation system. *IEEE Transactions on Mechatronics*, submitted.

Falangas, E.T., Dworak, J.A., and Koshigoe, S. (1994). Controlling plate vibrations using piezoelectric actuators. *Control System IEEE*, 14(4), 34–41.

Franklin, G., Powell, D., and Workman, M. (1997). *Digital Control of Dynamic Systems*. Prentice Hall.

Giaime, J., Saha, P., Shoemaker, D., and Sievers, L. (1996). A passive vibration isolation stack for ligo: design, modeling, and testing. *Review of scientific instruments*, 67(1), 208–214.

Ito, S., Neyer, D., Pirker, S., Steininger, J., and Schitter, G. (2015). Atomic force microscopy using voice coil actuators for vibration isolation. *2015 IEEE International Conference on Advanced Intelligent Mechatronics (AIM)*, 470–475.

Kim, Y., Kim, S., and Park, K. (2009). Magnetic force driven six degree-of-freedom active vibration isolation system using a phase compensated velocity sensor. *Review of Scientific Instruments*, 80(4).

Masciotti, J.M., Lasker, J.M., and Hielscher, A.H. (2008). Digital lock-in detection for discriminating multiple modulation frequencies with high accuracy and computational efficiency. *IEEE Transactions on Instrumentation and Measurement*, 57(1), 182–189.

Munnig Schmidt, R., Schitter, G., Rankers, A., and van Eijk, J. (2014). *The Design of High Performance Mechatronics*. Delft University Press, 2nd edition.

Nestorovic, T. and Trajkov, M. (2013). Optimal actuator and sensor placement based on balanced reduced models. *Mechanical Systems and Signal Processing*, 36(2), 271–289.

Pirro, S. (2006). Further developments in mechanical decoupling of large thermal detectors. *Nuclear Instruments and Methods in Physics Research Section A: Accelerators, Spectrometers, Detectors and Associated Equipment*, 559(2), 672–674.

Preumont, A. (2012). *Vibration control of active structures: an introduction*, volume 50. Springer Science & Business Media.

Schneiders, M.G.E., van de Molengraft, M.J.G., and Steinbuch, M. (2003). Introduction to an integrated design

for motion systems using over-actuation. *Proceedings of the European Control Conference*.

Thier, M., Saathof, R., Csencsics, E., Hainisch, R., Sinn, A., and Schitter, G. (2015). Design and control of a positioning system for robot-based nanometrology. *at-Automatisierungstechnik*, 63(9), 727–738.

Ungar, E. and Gordon, C. (1983). Vibration criteria for microelectronics manufacturing equipment. *Proceedings of International Conference on Noise Control Engineering, Edinburgh, Scotland*, 487–490.